Occultation of a Compact Radio Source by Venus

R. Linfield
Tracking Systems and Applications Section

An occultation of the compact radio source P 0507+17 by Venus on July 19, 1988, was observed in Tidbinbilla, Australia at a frequency of 2.3 GHz. The purpose of this observation was to measure the position of Venus in the radio reference frame. When data from both ingress (Venus dayside) and egress (Venus nightside) were used to solve for the position of Venus in ecliptic longitude and latitude, the results were consistent with zero offsets from the nominal values, with an uncertainty of approximately 0.2 arcsec in both coordinates. By using the nightside data alone, a value of -0.026 ± 0.04 arcsec was obtained for the linear combination $\Delta\lambda + 0.51\Delta\beta$, where $\Delta\lambda$ and $\Delta\beta$ were the offsets from their nominal values of the ecliptic longitude and latitude of Venus.

Distortion of a vacuum Fresnel fringe pattern by the Venus troposphere, and especially by the Venus ionosphere, was observed. The dayside ionosphere of Venus caused very large distortions; the amplitude of the first Fresnel fringe in the ingress data was eight times larger than had been expected for an airless planet. The observed fringe patterns were modeled by using plausible ionospheres (i.e., consistent with spacecraft measurements of the Venus ionosphere and with solar extreme ultraviolet flux and solar wind pressure measurements at the occultation epoch). However, the range of Venus ionospheric profiles (electron density as a function of altitude) allowed by a priori constraints and by the occultation data was large (e.g., the ionopause height on the dayside was uncertain by a factor of two). This ionospheric uncertainty (particularly on the dayside) translated into a large position uncertainty (0.2 arcsec for the dayside and 0.04 arcsec for the nightside). If it had been possible to calibrate the Venus ionosphere by some external means, the accuracy in $\Delta\lambda$ and $\Delta\beta$ would have been 0.01 arcsec or better.

I. Introduction

Very long baseline interferometry (VLBI) observations of compact extragalactic radio sources have established a stable, inertial reference frame (the radio reference frame), with source positions known to approximately 1 mas [1,2]. The planetary reference frame is defined by the orbits of the Moon and the planets. These orbits are known to a variable accuracy (relative to the orbit of the Earth), ranging from 5 mas for Mars to 500 mas for Pluto [3]. The orientation of the orbit of the Earth relative to the radio reference frame is known to 5–10 mas [4]; the positions of

the planets in the radio frame will have errors at least that large. Furthermore, due to modeling uncertainties, such as unknown asteroid masses [5], the planetary reference frame has an unknown net rotation rate. The errors of the planetary orbits in the radio frame are therefore time-variable.

Accurate measurements of the positions of planets relative to compact radio sources would allow the planetary orbits to be calculated in the stable radio reference frame. The orbits determined in that frame would allow improved studies of solar system dynamics. In addition, improved knowledge of the positions of the planets in the radio frame would lead to better navigation of planetary spacecraft. VLBI observations can locate the position of a spacecraft on the sky in the radio frame [6]. The current accuracy of such measurements is in the 1- to 10-mas range. For most navigation purposes, the position of a spacecraft relative to a planet or natural satellite is needed. Determining the relationship between the planetary and radio reference frames would have immediate benefits for spacecraft navigation.

The epoch and duration of an occultation of a compact radio source by a solar system object are sensitive to the location of that object in the radio frame. The epoch of the midpoint of occultation (specifically, the mean of the epoch of geometric ingress and egress) is the time when that solar system object and the radio source have the same position along the direction of motion of the object (approximately the ecliptic longitude). The duration of the occultation determines their relative position perpendicular to the direction of motion (i.e., approximately the ecliptic latitude).

The Moon sweeps out a solid angle on the sky, which grows at a rapid rate (approximately 3 square degrees per day as seen from any given point on the Earth, or 30 square degrees per day when integrated over the surface of the Earth), and it therefore frequently occults strong compact radio sources. Lunar occultations were used extensively in the 1960s to measure the structure and positions of celestial radio sources [7,8]. However, the topography of the lunar surface introduces variations as large as 3 arcsec in the limb of the Moon. These variations are known to an accuracy of approximately 0.2 arcsec [9]. Astrometric measurements from lunar occultations (e.g., a measurement of 3C 273 [10]) are limited to this accuracy.

Planetary occultations are much less sensitive than lunar occultations to errors from topography because planets are so much farther from the Earth than the Moon. The potential astrometric accuracy is therefore better. However, because planets subtend a much smaller angular diameter than the Moon and move more slowly on the sky, they sweep across a much smaller solid angle of sky per unit time than does the Moon (e.g., this rate of solid angle coverage is a factor of approximately 3000 smaller for Mercury and Venus than for the Moon) and occult many fewer strong radio sources.

II. The Occultation of P 0507+17 by Venus: Event Parameters and Observations

The search for planetary occultation events has been described elsewhere [11]. It is briefly summarized here. The JPL Planetary Ephemeris DE200 [12] was used to search through several catalogs of compact radio sources to identify planetary occultation events. The radio source catalogs that were searched include the JPL Astrometric VLBI Catalog [1], a catalog of compact sources within 10 deg of the ecliptic [13], and the Very Large Array (VLA) Calibrator Catalog. The period from January 1, 1988, to January 1, 2000, was searched.

Based on the strength of the occulted radio source and the sensitivity of radio telescopes in the occultation region on the Earth, the most favorable event discovered in this search (by a substantial margin) was an occultation of P 0507+17 by Venus on July 19, 1988. The region on the Earth where this event was visible was quite restricted: southeastern Australia, New Zealand, and a portion of the South Pacific Ocean extending eastward to 110 deg W longitude. Outside this region, one or both of the following constraints were violated. The first constraint was that Venus must be above the horizon at the time of the event, as seen from a given location on the Earth. The second constraint was that this location on the Earth must pass inside the umbra (i.e., the source must pass inside the limb of Venus). The finite distance between the Earth and Venus makes the relative position of Venus and a background radio source a function of location on the Earth. For the Earth–Venus distance at the time of this occultation, the position of Venus on the sky varied by 38 arcsec across the surface of the Earth.

There were two large radio telescopes within the occultation region: a 64-m diameter antenna at Parkes, Australia (operated by the Commonwealth Scientific and Industrial Research Organization) and a 70-m diameter antenna (DSS 43) in Tidbinbilla, Australia (operated by the JPL Deep Space Network). Due to a minimum elevation limit of 30 deg for this antenna, the Parkes antenna could not observe this event, but the event was observed with DSS 43. Parameters of this event, as seen from Tidbinbilla, are given in Table 1.

Total power measurements were made in two channels of 12-MHz bandwidth (BW) each, centered at 2272 and 2284 MHz. The integration time for each measurement was 0.050 sec. The data for the 2284-MHz channel are shown in Figs. 1(a) and (b), for ingress and egress, respectively. The observing frequency was chosen to maximize the ratio of the flux density of P 0507+17 to the flux density of Venus. At 8.4 GHz (the other observing frequency band available at DSS 43), that ratio was lower by a factor of 12. When combined with the smaller primary antenna beamwidth at the higher frequency (which causes time-dependent pointing errors to be more serious), the ratio of time variations in the total system temperature (due to causes other than the occultation) to the antenna temperature of P 0507+17 was expected to be much larger at 8.4 GHz than at 2.3 GHz. As an example, if the mean direction of antenna pointing were correct, drifts of 10 arcsec would cause system temperature variations of ~0.6 K at 8.4 GHz, but only ~0.003 K at 2.3 GHz. If the mean direction of antenna pointing were offset from the source direction, the system temperature variations would be larger at both frequencies. The antenna temperature of P 0507+17 was approximately 0.8 K at both frequencies. The total system temperature (including Venus and P 0507+17) was approximately 36 K at 2.3 GHz.

The BW was chosen as a trade-off between maximizing the signal-to-noise ratio (SNR), which argued for high BW, and minimizing the attenuation of high-order Fresnel fringes (discussed in the next section), which argued for a small BW. The final astrometric accuracy was not limited by either SNR or attenuation of high-order Fresnel fringes.

The weather at Tidbinbilla at the time of the occultation was changing rapidly. During ingress, mostly clear weather resulted in a stable system temperature. The data shown in Fig. 1(a) have not been modified. However, during egress, heavy clouds caused large, nonlinear system-temperature drifts. Polynomials of system temperature versus time were fit to the midpoints of the fringes in the raw data (i.e., halfway between maxima and minima) and subtracted to give the results plotted in Fig. 1(b). Two quartic polynomials, one for each half of the time span in Fig. 1(b), were used. Because of concern that this polynomial system temperature subtraction process had introduced errors into the measured epochs of fringe maxima and minima, the following test was performed: A cubic polynomial was added to the curve plotted in Fig. 1(b). This polynomial was zero at both ends of the data span, with a peak–peak span of 1 K in between [larger, by a factor >10, than any expected deviation of the true light curve from Fig. 1(b)]. The changes in the epochs of the fitted fringe maxima and minima resulting from the addition of this cubic polynomial had a mean value of 0.06 sec, with a standard deviation of 0.10 sec. The mean time offset of 0.06 sec corresponded to an offset in ecliptic longitude of 0.001 arcsec.

III. Occultation Theory

The theory for lunar occultations of celestial radio sources has been well developed [14,8]. Fresnel diffraction theory (e.g., [15]) expresses the received power as an integral across the two-dimensional impact plane (geometry shown in Fig. 2). For the case where the curvature of the limb can be neglected (a good approximation for lunar occultations), the received monochromatic flux density $I(p,\nu)$ at frequency ν for an impact parameter p is

$$
\begin{aligned}
&I(p,\nu) \\
&= \frac{I_\infty(\nu)}{2}\left[\int_0^\infty du \int_{-\infty}^\infty dv \cos\left\{\frac{\pi}{2}\left[(u-\psi)^2+v^2\right]\right\}\right]^2 \\
&+ \frac{I_\infty(\nu)}{2}\left[\int_0^\infty du \int_{-\infty}^\infty dv \sin\left\{\frac{\pi}{2}\left[(u-\psi)^2+v^2\right]\right\}\right]^2
\end{aligned}
\tag{1}
$$

The parameters u and v are normalized coordinates (Fresnel units) in the impact plane: $u = x\sqrt{2\nu/cd}$ and $v = y\sqrt{2\nu/cd}$, where x and y are physical displacements (in the impact plane) perpendicular and parallel to the limb, respectively; c is the velocity of light; d is the distance from the Earth antenna to the impact plane; and ψ is the impact parameter, in Fresnel units ($\psi = p\sqrt{2\nu/cd}$). The phase term $(\pi/2)[(u-\psi)^2+v^2]$ in the sine and cosine functions is the excess geometric path length (in radians) from that point in the impact plane to the Earth antenna, relative to the length of the most direct ray path. The monochromatic flux density as $p \to \infty$ is $I_\infty(\nu)$ (i.e., the total unobscured flux density of the occulted source). The limits of integration can be changed to take into account the curvature of the limb.

For the case of negligible curvature of the limb and no atmosphere on the occulting object, the identity

$$
\int_0^\infty \cos\left(\frac{\pi}{2}x^2\right) dx = \int_0^\infty \sin\left(\frac{\pi}{2}x^2\right) dx = \frac{1}{2}
$$

can be used to simplify Eq. (1).

$$I(p,\nu) = \frac{I_\infty(\nu)}{2}\left[\left(\frac{1}{2}+C(\psi)\right)^2+\left(\frac{1}{2}+S(\psi)\right)^2\right] \quad (2)$$

where $C(\psi)$ and $S(\psi)$ are the standard Fresnel integrals:

$$C(\psi) \equiv \int_0^\psi \cos\left(\frac{\pi}{2}x^2\right) dx$$

$$S(\psi) \equiv \int_0^\psi \sin\left(\frac{\pi}{2}x^2\right) dx$$

Equation (2) represents the vacuum Fresnel light curve for a point source. For an observed lunar occultation of a very compact source, the observed light curve can be fitted to a vacuum Fresnel light curve with two source coordinates as adjustable parameters. For a resolved source, the one-dimensional brightness distribution (integrated along the direction parallel to the limb of the Moon) can be derived from the light curve [14].

For an occultation by a planet with an atmosphere, the calculation of the intensity at the Earth becomes more complex. The integration in Eq. (1) assumes a constant amplitude and phase across the impact plane, but an atmosphere will, in general, modify both the amplitude and the phase of an incoming wave front. A thin screen in the impact plane, which changes the phase and the amplitude of the incoming radiation, can be incorporated into the expression for $I(p,\nu)$

$$\begin{aligned} I(p,\nu) &= \frac{I_\infty(\nu)}{2}\left[\int_0^\infty du \int_{-\infty}^\infty dv\, A(u,v) \right. \\ &\quad \left. \times \cos\left\{\frac{\pi}{2}\left[(u-\psi)^2+v^2\right]+\phi(u,v)\right\}\right]^2 \\ &\quad + \frac{I_\infty(\nu)}{2}\left[\int_0^\infty du \int_{-\infty}^\infty dv\, A(u,v) \right. \\ &\quad \left. \times \sin\left\{\frac{\pi}{2}\left[(u-\psi)^2+v^2\right]+\phi(u,v)\right\}\right]^2 \end{aligned} \quad (3)$$

where $A(u,v)$ and $\phi(u,v)$ are the amplitude and phase of the screen at the location (u,v) in the impact plane. The normalization of $A(u,v)$ is such that $A(u,v) = 1$ in the absence of a screen.

Note that because the conversion from physical coordinates to Fresnel units is a function of ν, the intensity at a given physical impact parameter p will depend on ν, *independent of any spectral variations in the source.* The observed flux $I(p)$ for a bandpass response with shape $B(\nu)$ is

$$I(p) = \int_0^\infty I(p,\nu)B(\nu)d\nu \quad (4)$$

The fringe amplitude exhibited by $I(p)$ will be less than the monochromatic fringe amplitude, due to imperfect coherence (i.e., nonzero phase spread) across the passband. As p increases, the fringes at the ends of the passband get increasingly out of phase, and the fringe amplitude is damped more severely.

The attenuation factor for this data set (0.5-percent fractional bandwidth) reached 0.59 for the highest observed fringe (no. 83) on the ingress light curve and 0.94 for the highest observed fringe (no. 31) on the egress light curve. These attenuation factors were calculated by integrating $I(p,\nu)$ across the passband (assumed to be rectangular) for one each of the best-fitting ingress and egress light curves. The attenuation factor is defined as the ratio of fringe amplitude for the actual bandpass to the monochromatic fringe amplitude.

The distance between P 0507+17 and Venus was $\sim 10^{15}$ times larger than the Earth–Venus distance. Therefore, the path length from P 0507+17 was essentially constant across the impact plane. The geometric phase terms in the Fresnel integrals, $(\pi/2)\left[(u-\psi)^2+v^2\right]$, were determined entirely by the Earth–Venus distance.

For an occultation of a spacecraft that is either in orbit about Venus or making a close flyby, a very different situation occurs. In this case the path length from the spacecraft to different locations in the impact plane varies dramatically. This variation is so large that only a very small region in the impact plane contributes to the Fresnel integrals, and geometric optics are a good approximation. This use of geometric optics, combined with tracking the frequency of the spacecraft carrier signal (Doppler shifts due to changing refraction angles can be measured), allows spacecraft occultation light curves to be inverted [16]. The variation of refractivity N [$N \equiv (n-1)$, where n is the index of refraction] with altitude is thereby obtained. Dual-frequency observations of spacecraft occultations allow a

separation of the refractivity of the neutral and ionized atmosphere, and permit a determination of electron density as a function of altitude.

Reflection of radio waves occurs only for electron densities large enough that the plasma frequency is comparable to the frequency of radiation. The maximum electron density in the dayside ionosphere of Venus is typically $5 - 10 \times 10^5 \mathrm{cm}^{-3}$ [17], giving a plasma frequency of ~10 MHz, far below the 2.3-GHz observation frequency used for this experiment. Absorption at 2.3 GHz in the Venus atmosphere is significant at altitudes of 55 km and lower [18]. Absorption can be incorporated into Eq. (3) by using a value of $A(u, v)$ less than 1.0.

Refraction in the atmosphere is more of a problem. A low-refractivity atmosphere, in which ray paths experience very little lateral displacement (i.e., shift in position perpendicular to their original direction of propagation) during their passage, can be treated as a thin screen. The ionosphere of Venus (maximum displacement of 2.3-GHz ray paths of ~5 m) fulfills this criterion. However, the neutral atmosphere of Venus causes large displacements of radio waves. Below 35 km altitude, the radial refractivity gradient becomes so large that entering radio waves do not escape [19]. Ray paths that pass within a few kilometers of this altitude are displaced by tens or hundreds of kilometers in the impact plane before emerging from the troposphere.

In order to incorporate these large tropospheric effects into the Fresnel integrals, a hybrid geometric/physical optics approach was used. Geometric ray-tracing calculations were made for the Venus troposphere for a one-dimensional grid of impact parameter p: 47–110 km in 20-m increments (rays entering with an impact parameter less than 47 km are refracted inside the 35-km boundary and ultimately reach the surface of the planet). The ray tracing was performed from the point of entry into the troposphere (chosen as 110 km altitude, where the refractivity is less than 10^{-7}), past the true impact plane, to a shifted impact plane, (i.e., closer to the Earth in the occultation geometry and outside the Venus atmosphere for nearly all ray paths). A sample displaced impact plane is shown in Fig. 2(a). Two separate ray-tracing runs, with impact plane shifts of 1000 and 4000 km were performed. Altitude profiles of refractivity [20] and the 2.3-GHz absorption coefficient [18] were used in these ray tracings.

The amplitude on this shifted impact plane was less than the amplitude on the true impact plane due to two effects. The first was absorption in the troposphere; the amplitude reduction due to this effect was $e^{-\tau(p)}$, where $\tau(p)$ was the integrated optical depth for a ray with impa parameter p. The second effect was refractive amplitu loss. Because the refractivity of the Venus troposphe increases with depth, rays that were parallel when th entered the troposphere diverged. In particular, the se aration $\Delta x'$ in the shifted impact plane was greater tha the difference Δp in impact parameters, diluting the r diation (i.e., reducing its amplitude). The refractive an plitude loss was dp/dx', and this factor was multiplied b the absorptive amplitude loss $e^{-\tau(p)}$ to give the amplitu A at location x' in the shifted impact plane. The "scree phase" ϕ for use in Eq. (3) was the excess phase for th ray path: the difference between its actual phase and th phase it would have had at the shifted impact plane i the absence of an atmosphere. This phase was the sum a dielectric term $\int 2\pi\nu(n-1)ds/c$ and a geometric ter $\int 2\pi\nu(\sec\theta - 1)ds/c$, where ν is the frequency of radiatio (2.3 GHz) and θ is the angle between the ray path at tha point and its initial direction. Both integrals were calcu lated over the entire path length from the entry into th troposphere until the arrival at the shifted impact plan (Note that the dielectric term remained constant after th ray exited from the troposphere.) The exit angle fro the troposphere was also calculated in order to allow th ionospheric contribution to be added later.

For sufficiently small impact parameters ($p < 53$ km and $p < 47.4$ km for impact plane shifts of 1000 km an 4000 km, respectively), the ray paths had not emerge from the troposphere when they reached the shifted impac plane. Ray tracing for these ray paths continued until the exited from the troposphere. The following procedure wa used to derive values of amplitude A and phase ϕ to us in the Fresnel integrals for these impact parameters. Th value of A was the product of the refractive and absorp tive losses at the shifted impact plane. The value of ϕ wa the excess phase (the sum of the geometric and dielectri integrals) at the shifted impact plane, with one extra ter added. This extra term was the dielectric integral fro the shifted impact plane until exit from the troposphere (i.e., the integrated refractivity encountered by that ray after the shifted impact plane). As discussed below, use of 1000- and 4000-km shifts in the impact plane gave negligible differences in the theoretical occultation light curves. Therefore, it is believed that this hybrid geometric and physical optics approach was adequate.

IV. Data Reduction and Modeling

The analysis of the occultation data fell into three general tasks. The first task was to calculate $I(p)$ in the presence of the atmosphere of Venus. The second task was to

determine $p(t, \Delta\lambda, \Delta\beta)$, where t represents time and $\Delta\lambda$ and $\Delta\beta$ represent the Venus ephemeris/radio frame offsets in ecliptic longitude and ecliptic latitude. The third task was to combine these results to obtain a frame tie. The first task is described in Subsections IV.A–IV.D. The numerical integration technique is described in Subsection IV.A. The properties of the Venus ionosphere are summarized in Subsection IV.B. Modeling of the Venus ionosphere at the occultation epoch, by using the occultation data, is presented in Subsection IV.C. The Venus troposphere and its effect on the occultation data are described in Subsection IV.D. Subsection IV.E describes the calculation of $p(t, \Delta\lambda, \Delta\beta)$. The third task (solving for the frame tie) is presented in Section V.

A. Numerical Integrations

Equation (3) was used to calculate $I(p, \nu)$, and the bandpass attenuation factor (see Section III) was used to convert $I(p, \nu)$ to $I(p)$. The sine and cosine expressions were factored so that the integration over v was a function of u but not of ψ.

$$\int_0^\infty du \int_{-\infty}^{+\infty} dv A(u,v) \cos\left\{\frac{\pi}{2}\left[(u-\psi)^2 + v^2\right] + \phi(u,v)\right\}$$

$$= \int_0^\infty du \cos\left\{\frac{\pi}{2}(u-\psi)^2\right\}$$

$$\times \int_{-\infty}^{+\infty} dv A(u,v) \cos\left\{\frac{\pi}{2}v^2 + \phi(u,v)\right\}$$

$$- \int_0^\infty du \sin\left\{\frac{\pi}{2}(u-\psi)^2\right\}$$

$$\times \int_{-\infty}^{+\infty} dv A(u,v) \sin\left\{\frac{\pi}{2}v^2 + \phi(u,v)\right\}$$

An integration over v was then performed for a grid of 1000–2000 u values. A Simpson's rule numerical integration was used. The integration step size was chosen by performing trial runs in which the step size was reduced until the results converged. The numerical integration was truncated at $\psi = 5$ or at the ionopause, whichever was higher. Analytic expressions for large arguments (≥ 5) of the Fresnel integrals [21] were then used to complete the integrations. This procedure reduced the calculation of I to a one-dimensional numerical integration for each value of ψ.

The values of $A(u, v)$ and $\phi(u, v)$ in Eq. (3) were determined by the Venus troposphere and ionosphere. With negligible absorption or ray path displacement by the ionosphere, $A(u, v)$ was a function only of the troposphere. The ray-tracing results described above were used to specify $A(u, v)$ on the shifted impact plane. Due to refraction in the troposphere, $A(u, v)$ did not drop abruptly to zero at the physical limb of Venus, but instead remained positive (with decreasing magnitude) for a considerable distance "inside" the limb. For impact parameters small enough that the ray paths entered the troposphere, $\phi(u, v)$ was the sum of three terms. The first was the contribution from the ionosphere due to entry with the impact parameter p (the value of p corresponding to a given u and v was obtained from the troposphere ray tracing). The second was the contribution from the troposphere, and the third was the contribution from the ionosphere due to an exit from the troposphere at an angle derived from ray tracing. For larger impact parameters, $\phi(u, v)$ was derived solely from the ionosphere.

B. General Properties of the Venus Ionosphere

Both $A(u, v)$ and $\phi(u, v)$ were entirely determined by p, the variation of the refractivity N with altitude h in the troposphere, and the variation of electron number density n_e with altitude in the ionosphere (n_e was assumed to be a function only of h, although that function was very different on the dayside and nightside of Venus). The function $N(h)$ was assumed to be known and not time variable, although two modified $N(h)$ functions were briefly examined (discussed below). The function $n_e(h)$ has been measured many times from spacecraft occultations (e.g., [22]). It is known to depend strongly upon time and upon the solar zenith angle (SZA) on Venus (the SZA is the angle between the zenith and the Sun, as seen from a given location on Venus). Due to the very slow rotation of Venus, the dependence of $n_e(h)$ on the solar hour angle (other than that predicted from the SZA dependence) is very weak [23]. There were no spacecraft occultation measurements at or near the epoch of the P 0507+17 event, so little more than statistical information on the ionosphere was available. The SZA's on Venus at the points of geometric occultation were 58 deg at ingress and 122 deg at egress. Typical integrated electron densities for "horizontal" lines of sight through the ionosphere (i.e., those which do not intersect the planet) are $\sim 2\text{–}5 \times 10^{13}\text{cm}^{-2}$ for 58-deg SZA and $\sim 1\text{–}2 \times 10^{12}\text{cm}^{-2}$ for 122-deg SZA, which corresponds to 10–30 and 0.5–1.0 cycles of phase at 2.3 GHz, respectively. The effect of the day ionosphere on 2.3-GHz radio waves is therefore much larger than that of the night ionosphere, as is very evident by comparing Figs. 1(a) and 1(b).

As is the case for the ionosphere of the Earth, the Venus ionosphere is strongly time variable. The time scale for large variations of the night ionosphere is at least as short as 24 hours, and perhaps as short as 1 hour [24]. The nightside ionosphere has a peak electron density that is typically around 15,000 cm^{-3}, with variations of a factor >2 in either direction [25]. These variations are weakly correlated with solar wind pressure and almost uncorrelated with solar extreme ultraviolet (EUV) flux. The ionopause height varies from 200 to over 3500 km. The height of maximum electron density is remarkably constant: 142.2 ±4.1 km [26]. Transport of energetic ions from the dayside is believed to drive the night ionosphere [27]; this process is highly dynamic.

The dayside ionosphere is less variable than that of the nightside. Kliore and Mullin showed that the peak electron density can be predicted from the SZA and the solar EUV flux, with a scatter of only approximately 5 percent [28]. They found that the altitude of the peak electron density is 140 ±2 km. Brace et al. [29] have studied the height of the dayside ionopause. The ionopause height varies inversely with solar wind pressure. However, the scatter is large, especially at large SZA (>50 deg) and low solar wind pressure ($<3 \times 10^{-8}$ dynes/cm^2).

C. Modeling of the Venus Ionosphere by Using the Occultation Data

At the epoch of the P 0507+17 occultation, measurements from the Pioneer Venus Orbiter spacecraft gave a solar EUV flux of 1.12×10^{12} photons/cm^2/sec and a solar wind pressure of 1.6×10^{-8} dynes/cm^2.[1] Using the results from [28] and [29], the predicted maximum n_e at an SZA of 58 deg was 3.85×10^5 cm^{-3}, with an uncertainty of 2×10^4 to 3×10^4 cm^{-3}. The predicted ionopause height at an SZA of 58 deg was 950 km, with an uncertainty of 400–500 km. The a priori model for the dayside ionosphere used these values, along with the functional shape for $n_e(h)$ shown in [23]. The a priori uncertainties in the nightside ionosphere were so large that large ranges in ionospheric parameters were examined in the modeling. Once $n_e(h)$ was specified, the contribution of $\phi(u, v)$ from the ionosphere was calculated by a numerical integration perpendicular to the impact plane, for a grid of 1000–2000 p values.

These a priori ionospheric $n_e(h)$ profiles were then adjusted in order to optimize the agreement between the model and the fringe amplitudes of the observed light curves. Initially, the agreement between the model and the observed light curve was judged visually. After an approximate fit was achieved, a numerical agreement factor was used to fine-tune the models. The absolute antenna temperature was difficult to determine from the observations due to weather-induced system temperature variations. Therefore, peak–peak fringe amplitudes were used to guide the modeling process. The weather-induced system temperature variations were substantially slower than the fringe frequency, so that the peak–peak amplitudes appeared to be nearly unaffected. The amplitudes at the fringe peaks were determined with parabolic fits to the peak regions. This procedure effectively discarded data away from the vicinity of the peaks. The SNR was degraded as a result, but still contributed negligibly to the final frame tie uncertainty. The amplitudes between most pairs of adjacent peaks could be well represented by a sinusoid, so that very little information was lost by saving only the peak amplitudes and their epochs.

The numerical integration yielded I for a grid of p. Parabolic fits to the fringe maxima and minima from these integrations gave values of I and p at the peaks. The χ^2 agreement between the model and observed light curves was not used to adjust the models. The errors in the observed peak–peak dayside amplitudes, especially in the lowest order fringes, were much smaller than the disagreement between the model and observed amplitudes. The χ^2 agreement would have been dominated by the modeling error on the largest two or three fringes. Instead, an agreement factor AF was used, which gave less weight to the largest fringes:

$$AF \equiv \sum_i \frac{(amp_{obs} - amp_{mod})^2}{amp_{obs}}$$

In this equation amp_{obs} and amp_{mod} represent the observed and model (i.e., calculated) peak–peak fringe amplitudes. These fringe amplitudes are expressed as fractions of the total source antenna temperature (i.e., when the source is not near Venus on the sky), and therefore they are dimensionless. The sum in AF was performed over the peaks of all the observed fringes (83 on the dayside or 31 on the nightside, where one fringe is defined to include both a maximum and a minimum). In the sum, both peak–peak combinations were included (i.e., the differences between a minimum and *both* adjacent maxima were included). This dual sum was performed to help drive the model dayside light curve toward the observed ingress curve. The values of amp_{mod} were derived from $I(p)$ curves and were therefore independent of $\Delta\lambda$ and $\Delta\beta$. Only the epochs of the fringes depended on these two offsets.

[1] L. Brace, personal communication, Goddard Space Flight Center, Greenbelt, Maryland, 1991.

The optimum weighting scheme for calculating the agreement factor depended on the detailed nature of the ionospheric $n_e(h)$ profile errors, which were unknown. It also depended on the manner in which these $n_e(h)$ errors projected into the values of amp_{mod}, which was highly nonlinear. An alternate agreement factor AF_{alt} was therefore also calculated by using a different weighting scheme:

$$AF_{alt} \equiv \sum_i \frac{(amp_{obs} - amp_{mod})^2}{amp_{obs}^2}$$

AF and AF_{alt} gave similar results as to which of two model light curves was a better fit to the data, although AF gave greater weight to the strongest fringes than did AF_{alt}. The process of model adjustment (described below) used AF.

1. Egress: Night Ionosphere of Venus. For the night ionosphere, simple models were used. The primary ionospheric component was modeled with seven parameters: h_{min}, $n_{e_{max}}$, h_{peak}, n_{e_2}, h_2, l, and h_{max} ($h_{min} < h_{peak} < h_2 \leq h_{max}$). In this model, $n_e = 0$ for $h < h_{min}$, $n_e = n_{e_{max}}$ at $h = h_{peak}$, and $n_e = n_{e_2}$ at $h = h_2$. Linear interpolation was used for the electron density in the region $h_{min} < h \leq h_2$ (i.e., the electron density rose linearly from zero to a peak value at $h = h_{peak}$ and then fell linearly to a value n_{e_2} at $h = h_2$). For $h_2 < h < h_{max}$, $n_e = n_{e_2} e^{-(h-h_2)/l}$. For $h \geq h_{max}$, $n_e = 0$. For all models, $n_{e_2} < 0.3 n_{e_{max}}$. A second component, with a peak electron density <10 percent of that of the primary component, consisted of only four parameters, as h_{max} was constrained to equal h_2, with $n_{e_2} = 0$. For the primary component h_{peak} was chosen as 142 km (the mean value observed from spacecraft occultations) for most models. The second component was located at an altitude well above the main peak of the second component [i.e., $h_{min}(2) > h_2(1) + 50$ km, where $h_{min}(2)$ was the value of h_{min} for component 2 and $h_2(1)$ was the value of h_2 for component 1]. Varying the ten parameters [other than $h_{peak}(1)$] produced several model ionospheres which all fit the observed amplitudes equally well. The qualitative agreement with the observed light curve was quite good (Fig. 3), but there were differences in detail. Ionospheric models with h_{peak} for the primary component of 147 and 152 km produced equally good fits. The observed egress light curve does not appear to constrain this parameter.

2. Ingress: Day Ionosphere of Venus. None of these eleven-parameter ionosphere models gave even a qualitative agreement with the observed ingress (dayside) light curve, so a more complex ionosphere model was used. In this model, a table of electron densities n_{e_i} at 20–30 altitudes was used, with a cubic spline interpolation in the value of n_e between these altitudes. For both types of models (the simple nightside model and the spline dayside model) the fitting process was automated. The parameters (the ten parameters other than h_{peak} for the nightside, or the 20–30 n_{e_i} values for the dayside) were adjusted one at a time through a series of 2–6 values relative to the nominal value (e.g., −5 percent, −1 percent, +1 percent, and +5 percent) and the agreement factor was calculated each time. If any of these adjusted values reduced the agreement factor AF, the nominal value for that parameter was then changed. Typically, this process was repeated for 5–10 loops through the complete set of parameters. The calculation of the light curve (which was needed in order to calculate AF) for one set of parameters required approximately six minutes of CPU time on a SUN 4/390 computer. This strongly limited the possible ways of adjusting parameters and precluded a full least-squares solution. The fit to the dayside curve could probably have been improved if multiple n_{e_i} values had been adjusted simultaneously. The large spread in frame-tie offsets among models which all fit the observed light curves fairly well suggests that an improved fitting procedure would not have significantly improved the frame-tie result.

For most fits, h_{peak} (the altitude of maximum n_e) was fixed at 140 km, although two fits each were run with h_{peak} of 135 and 144 km. The value of $n_{e_{max}}$ was constrained to lie within $3 \times 10^4 \text{cm}^{-3}$ of $3.85 \times 10^5 \text{cm}^{-3}$. The major differences among different models were the ionopause height (a range of 500–1300 km) and the value of n_e at the ionopause (a range of 2×10^3 to 10^4cm^{-3}). A good (but not excellent) fit to the observed dayside light curve was obtained for several combinations of the two parameters. As for the nightside modeling, the quality of the fit did not depend on h_{peak} (at least within the range of values that are consistent with spacecraft measurements of this parameter). Two of the best fits are shown in Fig. 4.

The structure of the ingress light curve shortly before the flux density dropped to zero was complex. Some models of the dayside ionosphere yielded one or more fringes in the region with amplitude much smaller than that of any observed fringe. When matching fringes between the model and observed light curves in order to calculate AF, any fringes among the first ten with an amplitude less than 20 percent of the total flux density [$I_\infty(\nu)$] were ignored (this limit is equal to 0.16 K in antenna temperature). Such fringes are indicated with small arrows in Fig. 4. These fringes are believed to be due to insufficiencies in

the model, probably as a result of a limited set of parameters.

D. The Venus Troposphere

For both the dayside and nightside model fitting, the sensitivity to troposphere changes was studied. Replacing the entire region of the troposphere below 80 km altitude with an opaque absorber [i.e., setting $A(u, v)$ in Eq. (3) to zero] did not change the results at all. Below 80 km altitude, the tropospheric phase contribution changed so rapidly with the impact parameter that contributions from adjacent regions canceled nearly perfectly. Using the opaque absorber in the analysis reduced or eliminated two sources of uncertainty from the overall modeling procedure. First, uncertainties in the absorption coefficient were unimportant because measurable absorption occurs only below 55 km. Second, concerns about the accuracy of the hybrid geometric/physical optics approach to the troposphere were greatly reduced. Above 80 km altitude, the deflections of ray paths passing through the troposphere are small (100 m at 80 km, 10 m at 90 km). The deviations of the fully modeled troposphere from that of a phase screen approach were negligible.

Above approximately 85 km altitude, the refractivity of the troposphere is poorly known [20]. The refractivity at these altitudes is so low that the Doppler shift of a carrier signal during spacecraft occultations is too small to measure accurately. However, the integrated phase of the troposphere was sufficiently large in this region to affect the occultation light curve of P 0507+17.

A nominal troposphere for light-curve modeling [in the form of a polynomial $\log(N(h))$, where $N(h)$ was the refractivity as a function of altitude] was adopted from [20]. In addition, two alternate troposphere polynomials were each used for one additional model of both the dayside and nightside light curves. These two alternate polynomials were chosen to reflect the range of possible errors in the nominal curve. Table 2 lists refractivity values from these three polynomials.

The effect of these alternate troposphere models was small. Small adjustments in the ionosphere parameters (much smaller than their a priori uncertainties) brought the agreement factor down to nearly the same value as for the nominal troposphere. For the nightside ionosphere, the nominal and the thin tropospheres gave better fits (20–40 percent lower AF) than did the thick troposphere. For the dayside ionosphere, all three tropospheres gave equally good fits. The uncertainty in the ionosphere was too large to allow significant constraints on the troposphere fro this occultation data set.

The magnitude of the effects of the different atmc spheric components is illustrated by their effective angula shift in the position of Venus. This shift in the light curv was approximately 0.25 arcsec for the night ionosphere approximately 0.8 arcsec for the day ionosphere, and ap proximately 0.3 arcsec for the troposphere. Of these thre the tropospheric shift was the most accurately known.

E. Impact Parameter as a Function of Both Time an Frame-Tie Offsets

The calculation of the impact parameter p as a func tion of time and frame-tie offsets required knowledge o the orbits of the Earth and Venus, and of the Earth' rotation. The Planetary Ephemeris DE200 was used t calculate the relative geocentric positions of Venus an P 0507+17 for zero frame-tie offset. Because both DE20 and the JPL Astrometric Catalog are expressed in J2000 no precession corrections were needed. Because P 0507+1 and Venus were very close together on the sky, no aber ration corrections were needed. However, a general rela tivistic correction was needed due to the bending of ra paths in the solar potential from P 0507+17 to Venu (from Venus to the Earth, ray paths from Venus an from P 0507+17 were deflected by the same amount, s that no further shift in the relative position of Venus an P 0507+17 occurred). The magnitude of this correctio was 4.07 mas/$[d \tan(\omega/2)]$ = 8.8 mas. Here d is the dis tance in astronomical units between Venus and the Su and ω is the angle between the Sun and P 0507+17, a seen from Venus. The direction of this bending lay en tirely in ecliptic longitude (in the sense that the apparen position of P 0507+17 was shifted to lower longitudes).

The topocentric parallax (i.e., the shift in the appar ent relative positions of P 0507+17 and Venus relative to their geocentric positions) was 19.6 arcsec $\cos el$, where el represented the elevation of the two objects as seen from DSS 43. It was therefore necessary to know the Earth's orientation and rotation and the station position to a fractional accuracy better than 5×10^{-5} (320 meters or 10 arcsec) to ensure an error of <1 mas in the parallax correction. The station vector was precessed from coordinates of date to J2000.

The impact parameter p was calculated for every 1 sec of time during the ingress and egress intervals displayed in Fig. 1. These calculations were performed for several small frame-tie offsets $\Delta\lambda$ and $\Delta\beta$, in addition to $\Delta\lambda = \Delta\beta = 0$.

Polynomial fits to the tabulated difference in impact parameters for different frame-tie offsets gave $\partial p/\partial\Delta\lambda(t)$ and $\partial p/\partial\Delta\beta(t)$, where t represents time.

For frame-tie offsets that are small as compared with the angular size of Venus, the change $\Delta T_{N_\pm}$ in epoch of a Fresnel fringe (maximum: + or minimum: −) was

$$\Delta T_{N_\pm} = -\frac{\frac{\partial p}{\partial\Delta\lambda}\Delta\lambda + \frac{\partial p}{\partial\Delta\beta}\Delta\beta}{\frac{\partial p}{\partial t}}$$

$$= \frac{\partial T_{N_\pm}}{\partial\Delta\lambda}\Delta\lambda + \frac{\partial T_{N_\pm}}{\partial\Delta\beta}\Delta\beta \qquad (5)$$

All derivatives in Eq. (5) were evaluated at $\Delta\lambda = \Delta\beta = 0$ and $t = T_{N_+}$ or $t = T_{N_-}$. The expressions for $\partial T_{N_\pm}/\partial\Delta\lambda$ and $\partial T_{N_\pm}/\partial\Delta\beta$ for both ingress and egress are given in Table 3. Note that $\partial T_{N_\pm}/\partial\Delta\lambda$ was nearly independent of time, because the path of Venus on the sky was nearly along the ecliptic.

There were a large number of measured fringe maxima or minima (166 during ingress and 62 during egress). It was possible to perform a least-squares solution for both $\Delta\lambda$ and $\Delta\beta$ from any subset of two or more residual values $\Delta T_{N_\pm} \equiv T_{N_{\pm observed}} - T_{N_{\pm model}}$. However, the resulting values of $\Delta\beta$ and $\Delta\lambda$ were highly correlated for time spans shorter than a few hundred seconds. When residuals from both ingress and egress were used together in one fit, the correlation between $\Delta\beta$ and $\Delta\lambda$ was much lower. In particular, if data from both ingress and egress were used and distributed roughly symmetrically in time about the occultation midpoint, the correlation dropped to nearly zero. For such a data set, $\Delta\beta$ was determined by the event duration and $\Delta\lambda$ was determined by its mean epoch.

V. Frame-Tie Results

Residual values ΔT from the two best-fitting models for each of the day and night ionospheres are given in Table 4. Labels of "A" and "B" for the day ionosphere models and "1" and "2" for the night ionosphere models are used for later reference. All four of these models used the nominal Venus troposphere. The values of ΔT are given at intervals of 50 sec, with respect to the reference epochs listed in Table 3 (these reference epochs were within five seconds of the times of geometric occultation for $\Delta\lambda = \Delta\beta = 0$). By using epochs from ingress and egress of $t = \pm 150$ sec and ± 200 sec, a symmetrical solution set was obtained. These four epochs were therefore used to make least-squares frame-tie estimates, in which time residuals at all four epochs were given equal weight. The results are given in Table 5.

There is a large scatter among the four entries in Table 5. The mean values from these four solutions are $\Delta\lambda = +0.03$ arcsec and $\Delta\beta = +0.09$ arcsec, with standard deviations of 0.11 arcsec for both parameters. These standard deviations are clearly only a very crude estimate of the true error. The range of allowed solutions includes $\Delta\lambda = \Delta\beta = 0$, with an error of approximately 0.2 arcsec.

The scatter in $\Delta\lambda$ and $\Delta\beta$ was dominated by uncertainty in the dayside ionosphere. By using egress data alone (this is equivalent to giving very low weight to the ingress data), a more accurate result was obtained. Because $\Delta\lambda$ and $\Delta\beta$ were highly correlated for solutions using just the egress data, a linear combination was used. The combination $\Delta\lambda + 0.51\Delta\beta$ was chosen because $\partial T_{N_\pm}/\partial\Delta\lambda$ and $0.51\,(\partial T_{N_\pm}/\partial\Delta\beta)$ were equal at the midpoint epoch (+150 sec) of the egress data set. A least-squares solution for $\Delta\lambda + 0.51\Delta\beta$ from the two sets of night residuals given in Table 4 yielded -0.026 ± 0.030 arcsec. As this estimate was based on only two model ionospheres, a more conservative error of 0.040 arcsec was adopted.

Model fits with the thin or thick troposphere models gave residual times ΔT that differed from nominal troposphere results by approximately 1 sec for ingress and <0.5 sec for egress. If it had been possible to somehow calibrate the Venus ionosphere, the errors in the frame-tie offsets due to tropospheric uncertainty would have been at least as small as those calculated for the night ionosphere (i.e., $\leq$0.01 arcsec, equivalent to 0.5 sec).

VI. Conclusions

"Light curves" of 2.3 GHz from both ingress and egress were obtained for the occultation of P 0507+17 by Venus. By comparing model light curves with the observed light curves for both ingress and egress, the frame-tie offsets $\Delta\lambda$ and $\Delta\beta$ (ecliptic longitude and latitude) were determined. The shape and strength of the Venus ionosphere were constrained by a priori information and by the requirement that the observed and model light curves have the same shape. Despite these constraints, uncertainty in the Venus ionosphere was the dominant error source for the frame-tie measurement. The next-largest error was due to uncertainty in the upper troposphere (altitude >85 km) of

Venus; the contribution from this error source was approximately a factor of 10 smaller than that from ionospheric uncertainty.

The solution for both $\Delta\lambda$ and $\Delta\beta$ gave results consistent with zero offsets, but with an error of approximately 0.2 arcsec. Using the egress (nightside) light curve alone (i.e., discarding data with large systematic errors) yielded higher accuracy for a linear combination of $\Delta\lambda$ and $\Delta\beta$: $\Delta\lambda + 0.51\Delta\beta = -0.026 \pm 0.04$ arcsec. Techniques other than occultations promise higher accuracy. VLBI observations of the Magellan spacecraft, now in orbit about Venus, have been performed, and are expected to yield a frame-tie accuracy of better than 0.01arcsec.[2] Radio occultations would appear to have useful astrometric potential only for planetary bodies with negligible ionospheres.

[2] C. Hildebrand, personal communication, Jet Propulsion Laboratory, Pasadena, California, 1991.

Acknowledgments

The author thanks J. Reynolds for extensive help with the data taking, and R. Treuhaft and X X Newhall, who made many useful suggestions based on a reading of a draft of this article.

References

[1] O. J. Sovers, C. D. Edwards, C. S. Jacobs, G. E. Lanyi, K. M. Liewer, and R. N. Treuhaft, "Astrometric Results of 1978–1985 Deep Space Network Radio Interferometry: The JPL 1987-1 Extragalactic Source Catalog," *The Astronomical Journal*, vol. 95, no. 6, pp. 1647–1658, 1988.

[2] C. Ma, D. B. Schaffer, C. De Vegt, K. J. Johnston, and J. L. Russell, "A Radio Optical Reference Frame, Part 1: Precise Radio Source Positions Determined by Mark III VLBI, Observations From 1979 to 1988 and a Tie to the FK5," *Astron. J*, vol. 99, no. 4, pp. 1284–1298, April 1990.

[3] E. M. Standish, "Celestial Reference Frames: Definitions and Accuracies," in *The Impact of VLBI on Astrophysics and Geophysics*, IAU Symposium no. 129, edited by M. J. Reid and J. M. Moran, Boston: Kluwer Academic Publishers, pp. 309–315, 1988.

[4] M. H. Finger and W. M. Folkner, "A Determination of the Radio-Planetary Frame Tie and the DSN Tracking Station Locations," AIAA paper 90–2905, presented at the AIAA/AAS Astrodynamics Conference, Portland, Oregon, August 20–22, 1990.

[5] J. G. Williams, "Determining Asteroid Masses from Perturbations on Mars," *Icarus*, vol. 57, p. 1, 1984.

[6] J. S. Border, F. F. Donivan, S. G. Finley, C. E. Hildebrand, B. Moultrie, and L. J. Skjerve, "Determining Spacecraft Angular Position with Delta VLBI: The Voyager Demonstration," AIAA Paper 82-1471, presented at the 1982 AIAA Conference, San Diego, California, August 1982.

[7] M. H. Cohen, "High-Resolution Observations of Radio Sources," *Annual Reviews of Astronomy and Astrophysics*, vol. 7, pp. 619–664, 1969.

[8] C. Hazard, "Lunar Occultation Measurements," in *Methods of Experimental Physics*, vol. 12C, edited by M. L. Meeks, New York: Academic Press, pp. 92–117, 1976.

[9] C. B. Watts, *Astronomical Papers of the American Ephemeris and Nautical Almanac*, vol. 17, Washington, DC; Government Printing Office, 1963.

[10] C. Hazard, J. Sutton, A. N. Argue, C. M. Kenworthy, L. V. Morrison, and C. A. Murray, "Accurate Radio and Optical Positions of 3C273B," *Nature Physical Science*, vol. 233, pp. 89–91, October 4, 1971.

[11] R. P. Linfield, "Using Planetary Occultations of Radio Sources for Frame-Tie Measurements, Part 1: Motivation and Search for Events," *TDA Progress Report 42-103*, vol. July–September 1990, Jet Propulsion Laboratory, Pasadena, California, pp. 1–13, November 15, 1990.

[12] E. M. Standish, "Orientation of the JPL Ephemerides, DE 200/LE 200, to the Dynamical Equinox of J 2000," *Astronomy and Astrophysics*, vol. 114, pp. 297–302, 1982.

[13] A. E. Wehrle, D. D. Morabito, and R. A. Preston, "Very Long Baseline Interferometry Observations of 257 Extragalactic Radio Sources in the Ecliptic Region," *The Astronomical Journal*, vol. 89, pp. 314–336, 1984.

[14] P. A. G. Scheuer, "On the Use of Lunar Occultations for Investigating the Angular Structure of Radio Sources," *Australian Journal of Physics*, vol. 15, no. 2, pp. 332–343, 1962.

[15] M. Born and E. Wolf, *Principles of Optics*, Elmsford, New York: Pergamon Press, pp. 370–434, 1964.

[16] V. R. Eshleman, G. Fjeldbo, and A. Kliore, "The Neutral Atmosphere of Venus as Studied with the Mariner V Radio Occultation Experiments," *Astronomical Journal*, vol. 76, pp. 123–140, 1971.

[17] S. J. Bauer, L. M. Brace, H. A. Taylor, Jr., T. K. Breus, A. J. Kliore, W. C. Knudsen, A. F. Nagy, C. T. Russell, and N. A. Savich, "The Venus Ionosphere," *Advances in Space Research*, vol. 5, no. 11, pp. 233–267, 1985.

[18] J. M. Jenkins and P. G. Steffes, "Results for 13-cm Absorptivity and H_2SO_4 Abundance Profiles From the Season-10 (1986) Pioneer Venus Orbiter Radio Occultation Experiment," *Icarus*, vol. 90, pp. 129–138, 1991.

[19] V. S. Avduevsky, M. Y. Marov, and M. K. Rozhdestvensky, "Model of the Atmosphere of the Planet Venus Based on Results of Measurements Made by the Soviet Automatic Interplanetary Station Venera 4," *Journal of The Atmospheric Sciences*, vol. 25, pp. 537–545, 1968.

[20] A. Seiff, J. T. Schofield, A. J. Kliore, F. W. Taylor, and S. S. Limaye, "Models of the Structure of the Atmosphere of Venus from the Surface to 100 Kilometers Altitude," in *The Venus International Reference Atmosphere, Advances in Space Research*, vol. 5, no. 11, pp. 3–58, 1985.

[21] M. Abramowitz and I. A. Stegun, *Handbook of Mathematical Functions*, New York: Dover Publications, p. 322, 1985.

[22] T. E. Cravens, A. J. Kliore, J. U. Kozyra, and A. F. Nagy, "The Ionospheric Peak on the Venus Dayside," *Journal of Geophysical Research*, vol. 86, pp. 11,323–11,329, 1981.

[23] R. F. Theis, L. H. Brace, and H. G. Mayr, "Empirical Models of the Electron Temperature and Density in the Venus Atmosphere," *Journal of Geophysical Research*, vol. 85, pp. 7787–7794, December 30, 1980.

[24] L. H. Brace, T. I. Gombosi, A. J. Kliore, W. C. Knudsen, A. F. Nagy, and H. A. Taylor, "The Ionosphere of Venus Observations and Their Interpretation," in *Venus*, edited by D. M. Hunten, L. Colin, T. M. Donahue, and V. I. Moroz, Tucson: University of Arizona Press, pp. 779–840, 1983.

[25] L. H. Brace, R. F. Theis, and J. D. Mihalov, "Response of Nightside Ionosphere and Ionotail of Venus to Variations in Solar EUV and Solar Wind Dynamic Pressure," *Journal of Geophysical Research*, vol. 95, pp. 4075–4084, April 1, 1990.

[26] A. J. Kliore, I. R. Patel, A. F. Nagy, T. E. Cravens, and T. I. Gombosi, "Initial Observations of the Nightside Ionosphere of Venus from Pioneer Venus Orbiter Radio Occultations," *Science*, vol. 205, pp. 99–102, July 6, 1979.

[27] L. H. Brace, R. F. Theis, H. B. Niemann, H. G. Mayr, W. R. Hoegy, and A. F. Nagy, "Empirical Models of the Electron Temperature and Density in the Nightside Venus Ionosphere," *Science*, vol. 205, pp. 102–105, July 6, 1979.

[28] A. J. Kliore, J. Arvydas, and L. F. Mullen, "The Long-Term Behavior of the Main Peak of the Dayside Ionosphere of Venus During Solar Cycle 21 and Its Implications on the Effect of the Solar Cycle Upon the Electron Temperature in the Main Peak Region," *Journal of Geophysical Research*, vol. 94, pp. 13,339–13,351, October 1, 1989.

[29] L. H. Brace, R. F. Theis, W. R. Hoegy, J. H. Wolfe, J. D. Mihalov, C. T. Russell, R. C. Elphic, and A. F. Nagy, "The Dynamic Behavior of the Venus Ionosphere in Response to Solar Wind Interactions," *Journal of Geophysical Research*, vol. 85, pp. 7663–7678, December 30, 1980.

Table 1. Parameters of July 19, 1988, occultation by Venus as seen from Tidbinbilla, Australia.

Parameter	Value
P 0507+17 position	
Right ascension, J2000	05 10 02.3691
Declination, J2000	18 00 41.581
Flux density of P 0507+17	
2.3 GHz	1.0 Jy
8.4 GHz	1.0 Jy
Flux density of Venus	
2.3 GHz	2.4 Jy
8.4 GHz	30 Jy
Approximate midpoint of occultation	UT 19:58
Approximate duration of occultation	19 min
Elevation of Venus at midpoint	18 deg
Angle between Venus and the Sun (as seen from the Earth)	40 deg
Distance from Earth to Venus	67.5×10^6 km
Angular diameter of Venus	37 arcsec
Angular velocity of Venus	1.21 arcsec/min

Table 2. Troposphere refractivity values used in light-curve modeling.

Altitude, km	$\log_{10} N$		
	Nominal	Thin	Thick
80	−5.4	−5.4	−5.4
85	−6.0	−6.0	−6.0
90	−6.6	−6.9	−6.4
95	−7.1	−8.0	−6.6
100	−7.7	−9.1	−6.8
105	−8.2	−10.1	−7.1
110	−8.8	−10.8	−7.4

Table 3. Dependence of fringe epochs upon frame-tie offsets.

Quantity	Constant coefficient	Linear coefficient	Quadratic coefficient
Ingress $\partial T_{N_\pm}/\partial\Delta\lambda$	−48.4	+0.003	
Ingress $\partial T_{N_\pm}/\partial\Delta\beta$	−71.7	−0.124	-2.1×10^{-4}
Egress $\partial T_{N_\pm}/\partial\Delta\lambda$	−53.4	+0.002	
Egress $\partial T_{N_\pm}/\partial\Delta\beta$	+67.2	−0.121	$+2.0 \times 10^{-4}$

Note: Reference times for the polynomials are 19:48:50 for ingress and 20:07:42 for egress. Units for $\Delta\lambda$ and $\Delta\beta$ are arcseconds, and units for T_N are seconds.

Table 4. Fringe epoch residuals for the best-fitting models.

Model	−150 sec	−200 sec	−250 sec	−300 sec
Day A	−18 sec	−14 sec	−14.5 sec	−16 sec
Day B	+ 7 sec	0 sec	− 5.5 sec	− 9 sec

Model	+100 sec	+150 sec	+200 sec
Night 1	−1.3 sec	+1 sec	+1.3 sec
Night 2	+4.4 sec	+4.8 sec	+4.6 sec

Table 5. Frame-tie offsets.

Model combination	$\Delta\lambda$, arcsec	$\Delta\beta$, arcsec
A1	+0.14	+0.16
A2	+0.10	+0.19
B1	−0.04	−0.02
B2	−0.08	−0.01

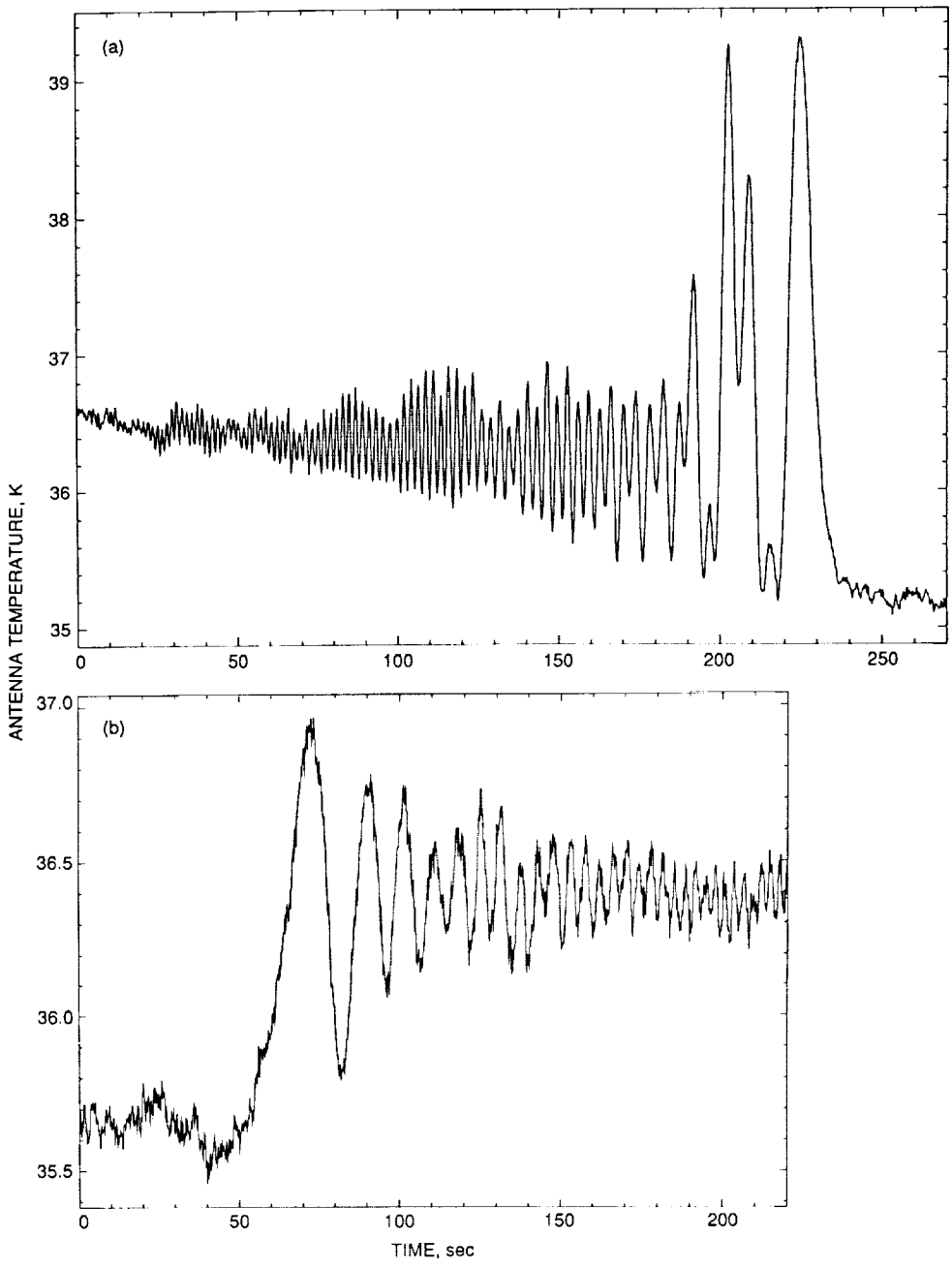

Fig. 1. Observed light curves for the occultation of P 0507+17 by Venus. The data were taken with the 70-m DSN antenna at Tidbinbilla, at a frequency of 2.3 GHz: (a) ingress light curve (dayside of Venus) and (b) egress light curve (nightside of Venus).

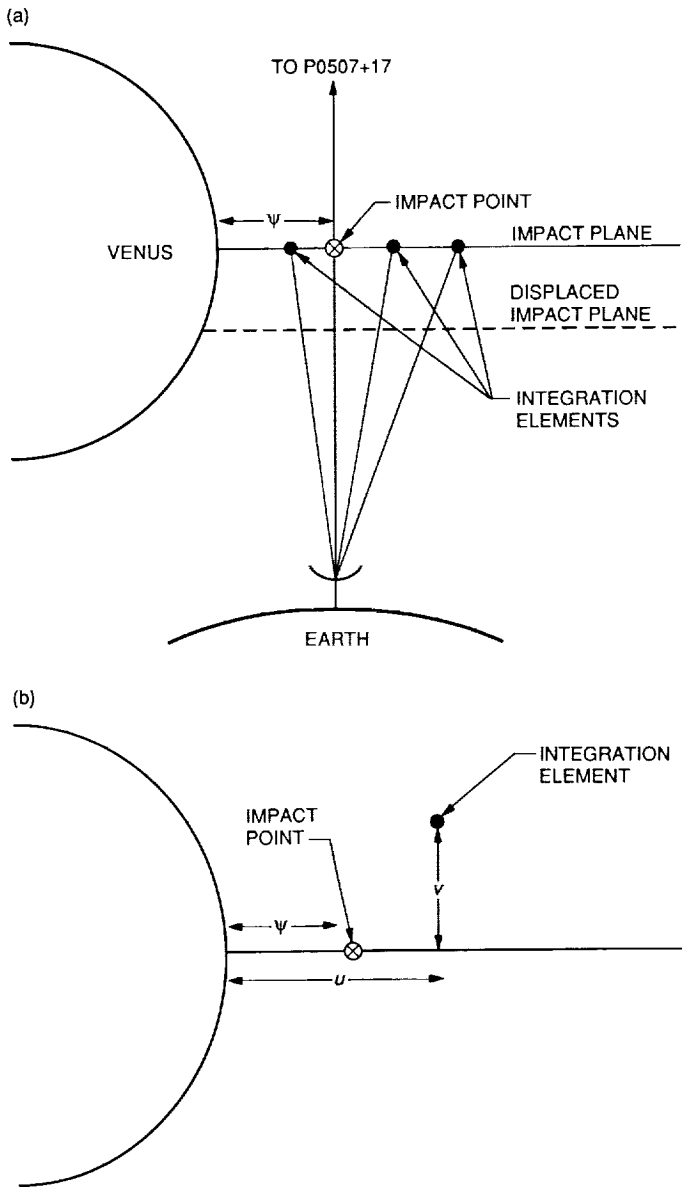

Fig. 2. Geometry for occultation calculations for (a) the observer-source dimension and one dimension in the impact plane. Note the impact point, the three integration elements (for Fresnel integrals) in the impact plane, and a sample displaced impact plane (discussed in the text). (b) The two-dimensional impact plane. Both u and v represent the coefficients (in Fresnel units) of the integration element, and ψ represents the impact parameter.

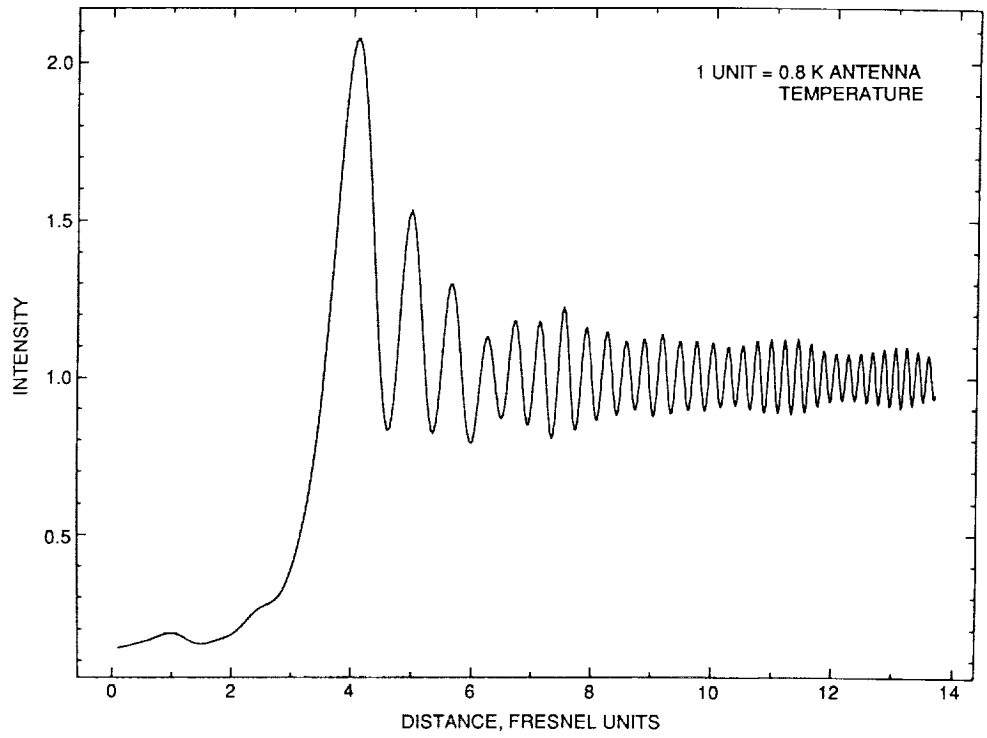

Fig. 3. One of the best-fitting model light curves for the egress (nightside) data.

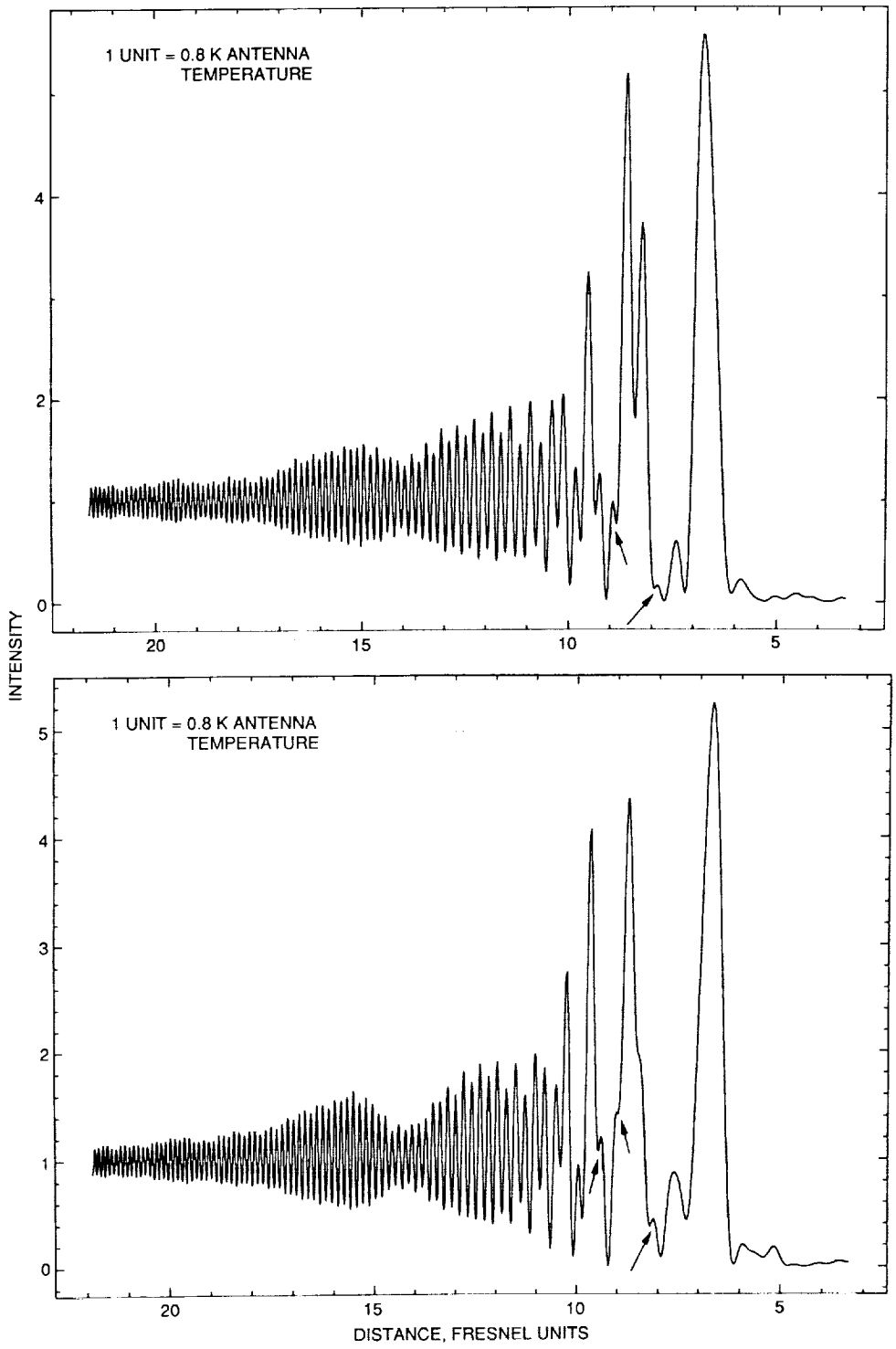

Fig. 4. Two of the best-fitting model light curves for the ingress (dayside) data. The tiny fringes marked with arrows were ignored when calculating residual fringe epochs, as discussed in the text.